

Merger Driven or Internal Evolution? A New Morphological Study of Tidal Disruption Event Host Galaxies

JANET N.Y. CHANG ^{1,2} CONNOR BOTTRELL ³ LIXIN DAI ^{1,2} RUDRANI KAR CHOWDHURY ^{1,4} MENG GU ^{5,2}
RENBIN YAN ^{6,7} LEONARDO FERREIRA ^{8,9} SARA L. ELLISON ⁸ SCOTT WILKINSON ⁸ AND THOMAS DE BOER ¹⁰

¹*Department of Physics, The University of Hong Kong
Pokfulam Road, Hong Kong, China*

²*The Hong Kong Institute for Astronomy and Astrophysics, The University of Hong Kong
Pokfulam Road, Hong Kong, China*

³*International Centre for Radio Astronomy Research, University of Western Australia
35 Stirling Hwy, Crawley, WA 6009, Australia*

⁴*Tata Institute of Fundamental Research, Homi Bhabha Road, Mumbai 400005, India*

⁵*Department of Astronomy, Tsinghua University
Beijing, China*

⁶*Department of Physics, The Chinese University of Hong Kong
Shatin, New Territories, Hong Kong, China*

⁷*CUHK Shenzhen Research Institute
No.10, 2nd Yuexing Road, Nanshan, Shenzhen, China*

⁸*Department of Physics and Astronomy, University of Victoria
Victoria, BC V8P 5C2, Canada*

⁹*Centre for Astronomy and Particle Theory, University of Nottingham
Nottingham, UK*

¹⁰*Institute for Astronomy, University of Hawaii
2680 Woodlawn Drive, Honolulu, HI 96822, USA*

ABSTRACT

Host galaxies of tidal disruption events (TDEs) show enhanced central stellar concentration and are preferentially found in post-starburst and green valley populations. This connection has led to the proposal that TDE host galaxies likely have gone through recent mergers. We conduct a new morphological study of 14 TDE host galaxies, using the r -band images from Sloan Digital Sky Survey (SDSS), Dark Energy Camera Legacy Survey (DECaLS), and Ultraviolet Near-Infrared Optical Northern Survey (UNIONS), with the images from the latter two surveys having much higher depth and resolution than SDSS. We examine galaxy structures using conventional methods and also apply diagnostics of merger activity from suite of machine learning models. Consistent with previous studies, our results show that TDE host galaxies are $\sim 16\%$ more centrally concentrated when compared to non-TDE-host controls. However, surprisingly, TDE hosts lack any indication of recent merger activity from both morphological analysis and our machine learning merger classifier. Instead, our results reveal that TDE host galaxies are approximately 1.5 to 2.5 times more likely to have bar-like or ring-like structures than their controls. This enhancement is even more prominent for TDEs in the green valley, with the factor reaching almost 3. Based on these results, we propose that bar-driven secular evolution, instead of mergers, likely dominates the recent evolution of TDE hosts found in the green valley, which can simultaneously explain their distinctive nuclear properties and enhanced TDE rates.

Keywords: Tidal disruption event, host galaxies, stellar structure, post-starburst galaxies, green valley galaxies, galaxy morphology, galaxy merger, secular evolution, galactic bars

1. INTRODUCTION

A tidal disruption event (TDE) occurs when a star ventures near a massive black hole (MBH) and is torn apart

by tidal forces (M. J. Rees 1988). Approximately half of the stellar debris remains bound to the MBH, forming an accretion disk that produces a luminous flare through collision and subsequent accretion processes (C. R. Evans & C. S. Kochanek 1989; C. Bonnerot & N. C. Stone 2021; J. L. Dai et al. 2021; E. M. Rossi et al. 2021). TDEs offer a distinct opportunity to probe MBH demographics and gain insights into black hole (BH) accretion physics (S. van Velzen et al. 2021). In recent years, the TDE detection rate has rapidly increased due to advancements in instrumentation (S. Gezari 2021; E. Hammerstein et al. 2023). This surge has sparked growing interest in TDEs. A complete understanding of TDE astrophysics therefore requires characterizing both their host galaxy environments and the selection biases inherent to different observational surveys (K. D. French et al. 2016; J. Law-Smith et al. 2017). Upcoming surveys like Rubin/LSST will deliver a vast sample of TDEs, further emphasizing the need to advance our understanding of these events (K. Bricman & A. Gomboc 2018; S. Gezari et al. 2018).

Previous studies have revealed that TDE host galaxies are statistically distinct from the general galaxy population when matched on stellar mass and redshift. They exhibit: (1) higher central stellar concentrations (J. Law-Smith et al. 2017; O. Graur et al. 2018), (2) greater prevalence in the green valley (GV) (J. Law-Smith et al. 2017; E. Hammerstein et al. 2021; Y. Yao et al. 2023), and (3) over-representation among E+A (post-starburst) galaxies, which are systems with weak $H\alpha$ emission (indicating suppressed star formation) and strong Balmer absorption (signaling a recent starburst) (K. D. French et al. 2016; O. Graur et al. 2018).

The physical characteristics of TDE host galaxies likely have intrinsic connections to TDE rates. The occurrence rate of TDEs is fundamentally governed by stellar dynamics in galactic nuclei, where stars interact through processes such as two-body relaxation (J. Wang & D. Merritt 2004). During these dynamical processes, the nuclear stellar structure, including the stellar population and density profiles, plays a critical role in setting the TDE rate (N. C. Stone et al. 2020; H. Pfister et al. 2020; J. N. Y. Chang et al. 2025). These works demonstrate that denser stellar environments in the vicinity of MBHs naturally enhance TDE rates.

Galaxy mergers have been suggested as a compelling mechanism to explain some of these observed properties of TDE host galaxies (K. D. French et al. 2020b). Major mergers can distort galaxy shapes through tidal forces, drive radial gas inflows and disrupt stellar rotation (D. Lynden-Bell 1967; A. Toomre 1977; R. De Propris et al. 2007; P. F. Hopkins et al. 2013; D. R. Patton

et al. 2016a). This triggers central starbursts and MBH accretion (L. Hernquist 1989; M. Sparre & V. Springel 2016; F. Renaud et al. 2022; S. Byrne-Mamahit et al. 2023, 2024; L. Ferreira et al. 2025) and stellar bulge growth (A. Brooks & C. Christensen 2016; S. L. Ellison & L. Ferreira 2025), thereby enhancing nuclear stellar densities. The energetic feedback following episodes of significantly enhanced central star formation and MBH accretion in major mergers is also a compelling pathway for making post-starburst galaxies (S. L. Ellison et al. 2022; S. Quai et al. 2023; S. Ellison et al. 2024). Interestingly, H. Pfister et al. (2019) incorporated basic TDE physics into a galaxy merger simulation and found that the TDE rates can indeed increase by orders of magnitude at certain phases after mergers.

It is expected that mergers should leave detectable signatures in galaxy structure such as tidal tails or asymmetric features (A. Toomre & J. Toomre 1972; J. E. Barnes & L. Hernquist 1998; C. J. Conselice 2003; J. M. Lotz et al. 2008). Various studies have searched for observational evidence of mergers in the current sample of TDE host galaxies, but none have obtained conclusive evidence. For example, J. Law-Smith et al. (2017) found no significant enhancement in asymmetry among their sample of 10 TDE hosts using Sloan Digital Sky Survey (SDSS) imaging (K. N. Abazajian et al. 2009). However, this analysis was limited by the small TDE sample size, SDSS relatively shallow depth, and poor spatial resolution, which could make faint merger signatures hard to detect (S. Wilkinson et al. 2024). K. D. French et al. (2020b) later examined 4 TDE hosts using higher-resolution HST imaging but similarly found no evidence for recent mergers.

While galaxy mergers remain a compelling scenario, other evolutionary pathways should also be considered to account for the unique characteristics of TDE host galaxies. Simulations and observations support the diversity of quenching pathways: T. A. Davis et al. (2019) find that post-starburst galaxies arise from a variety of mechanisms, including but not dominated by major mergers, while M. M. Pawlik et al. (2019) show that only a minority of post-starburst galaxies follow the classic “blue-to-red” merger track, with many experiencing star-formation truncation without a dominant starburst. This opens the door for slower, less disruptive processes to be important mechanisms for creating galaxies with specific properties. In particular, secular evolution, which is the gradual, internal transformation in relatively isolated galaxies, can also enhance galaxy nuclear stellar densities despite being a much less violent process compared to galaxy mergers (J. Kormendy & R. C. Kennicutt 2004). Unlike mergers, secular evo-

lution often preserves axisymmetric galaxy structures, providing an alternative route to the dense stellar cores favorable for TDEs.

In the study presented here, we conduct a detailed morphological analysis of TDE host galaxies to determine whether their observed structures are more consistent with recent merger activity or alternative mechanisms such as secular evolution. For this study, higher-quality galaxy images are crucial, as previous work has demonstrated that merger features become undetectable as image quality deteriorates (C. Bottrell et al. 2019; R. McElroy et al. 2022; S. Wilkinson et al. 2024). We leverage the unprecedented sample size of the Sloan Digital Sky Survey (SDSS; D. G. York et al. 2000) and the exceptional capabilities of the Dark Energy Camera Legacy Survey (DECaLS) and Ultraviolet Near-Infrared Optical Northern Survey (UNIONS; S. Gwyn et al. 2025). In particular, observations conducted using the Canada-France-Hawaii Telescope (CFHT) on Maunakea provide an excellent combination of depth, resolution, and wide-area coverage in the r -bands. These high-quality optical images have a strong record of revealing faint tidal features and disturbed morphologies (R. W. Bickley et al. 2021; S. Wilkinson et al. 2022; L. Ferreira et al. 2024), providing key signatures of recent galaxy interactions that may enhance TDE rates. To maximize the scientific return from UNIONS’ superb data, we also combine these images with comprehensive structural measurements from S. Wilkinson et al. (2022) and merger classifications based on a hybrid machine learning approach (L. Ferreira et al. 2024, 2026).

The paper is structured as follows. We provide a description of the methodology in Section 2, where we introduce the imaging surveys we utilized, the details of the morphological parameters and classification method, our sample of TDE host galaxies, their control sample, the identifications of rings and bars structures, and the boundary of the star-forming main sequence. We compare broad physical properties of TDE host galaxies to non-TDE hosts in Sec. 3.1, contrast stellar concentration in Sec. 3.2, and merger indicators in Sec. 3.3 and Sec. 3.4, respectively. We then investigate the fraction of bars and rings in these galaxies in Sec. 3.5. We discuss the possible impact of bar-driven secular evolution on TDE host galaxies in Sec. 4 and summarize our results in Sec. 5.

2. METHODS AND DATA

2.1. Imaging Data

We obtain images from SDSS, DECaLS, and UNIONS. SDSS represents one of the most comprehensive astronomical surveys, combining both imaging and spectro-

scopic observations, while DECaLS and UNIONS offer deeper and higher-resolution images.

2.1.1. SDSS

SDSS is composed of imaging and spectroscopic surveys, carried out with a dedicated 2.5m telescope at the Apache Point Observatory in Southern New Mexico. Its imaging camera contains 30 CCDs, with a median r -band seeing of 1.32 arcsec and 5σ point source depth of 22.7 mag (D. G. York et al. 2000).

We utilized data from Data Release 7 (DR7; K. N. Abazajian et al. 2009), which includes data from three main surveys: the SDSS Legacy Survey, the Sloan Extension for Galactic Understanding and Exploration survey (SEGUE), and the SDSS Supernova survey. The DR7 imaging data cover approximately 8423 deg² of the legacy sky and 3240 deg² of the SEGUE sky, while the spectroscopic data span 8200 deg² of the sky.

2.1.2. DECaLS

DECaLS (R. D. Blum et al. 2016) is conducted using the Dark Energy Camera (DECam) located at the Cerro Tololo Inter-American Observatory. It is mounted on the Victor M. Blanco 4m telescope. It contains 74 CCDs and images a 3 deg² field of view, with an r -band depth of 23.4 mag. It covers 14000 square degrees in the g , r , and z bands. More importantly, it overlaps with SDSS in the region $-20 < \text{Dec} < +30\text{deg}$.

2.1.3. UNIONS

UNIONS (S. Gwyn et al. 2025) is a collaboration of wide field imaging surveys of the northern hemisphere. UNIONS consists of the Canada-France Imaging Survey (CFIS), conducted at the 3.6-meter CFHT on Maunakea, members of the Pan-STARRS team, and the Wide Imaging with Subaru HyperSuprime-Cam of the Euclid Sky (WISHES) team. CFHT/CFIS is obtaining deep u and r bands; Pan-STARRS is obtaining deep i and moderate-deep z band imaging, and Subaru is obtaining deep z -band imaging through WISHES and g -band imaging through the Waterloo-Hawaii IfA g -band Survey (WHIGS). These independent efforts are directed, in part, to securing optical imaging to complement the Euclid space mission, although UNIONS is a separate collaboration aimed at maximizing the science return of these large and deep surveys of the northern skies.

UNIONS achieves exceptional image quality with median r -band seeing of 0.6 arcseconds, more than twice as sharp as SDSS, and reaches an impressive 5σ depth of 25.3 mag, making it more sensitive to faint sources and structures compared to SDSS. UNIONS covers approximately 5,000 square degrees in r -band.

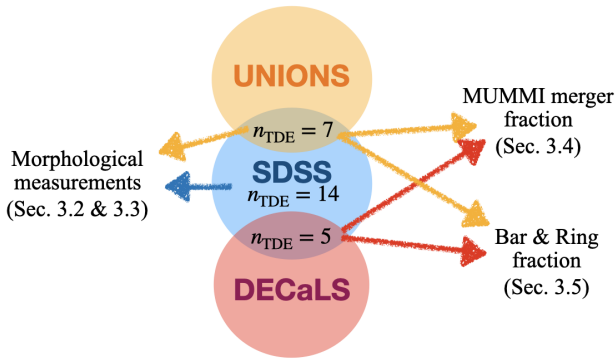


Figure 1. Schematic diagram illustrating the overlap of image catalogs used for various analyses. The central blue region represents the initial SDSS spectroscopic catalog (with a sample of 14 TDE host galaxies). Overlaid are the UNIONS (orange) and DECaLS (red) galaxies, showing their respective overlaps: 7 of the SDSS TDE hosts are also present in UNIONS, and 5 are also found in DECaLS. Color-coded arrows indicate which image catalog was utilized for each specific analysis discussed in Sec. 3.

UNIONS provides significant advantages over SDSS for studying galaxy morphology and evolution. Its superior image quality and greater depth enable the detection of faint tidal features and low-surface-brightness structures that are often unresolved in SDSS data. These improvements allow for more precise morphological measurements, particularly in the area of galaxies where merger signatures and secular processes leave subtle imprints. While UNIONS’ footprint is limited to $\text{Dec} > 30$ deg, it is complemented by DECaLS, which provides similar quality imaging for $\text{Dec} < 30$ deg. Therefore, the combined high-resolution imaging from UNIONS and DECaLS, paired with SDSS invaluable spectroscopic coverage, creates a powerful synergy that enhances our ability to investigate galaxy formation and dynamical evolution.

2.2. Measurements and Classification

In this section, we present the galaxy sample selection and derived properties for our TDE host analysis. As will be described in this section, we obtain a baseline sample of $n_{\text{SDSS}} = 585,016$ galaxies with basic derived properties and measurements. We utilize complementary datasets including: (1) morphological measurements of both SDSS and UNIONS images, and (2) merger classification by Multi Model Merger Identifier (MUMMI; L. Ferreira et al. 2024, 2026) on UNIONS and DECaLS images. In addition, we also utilize UNIONS and DECaLS images for bar and ring classification. Fig. 1 shows a schematic of the described data.

2.2.1. Morphological Measurements

We start with the SDSS DR7 catalog (M. A. Strauss et al. 2002). We include the star-formation rate (SFR) and velocity dispersion σ from the MPA-JHU catalog (J. Brinchmann et al. 2004), and total stellar mass M_* from J. T. Mendel et al. (2014). We consider only SDSS galaxies with $z > 0.001$ and $M_* > 10^8 M_\odot$. This results in a sample with size $n_{\text{SDSS}} = 585,016$.

We use morphology measurements from S. Wilkinson et al. (2022), computed with STATMORPH (V. Rodriguez-Gomez et al. 2019) and applied to both SDSS and UNIONS images. The concentration parameter C_{stat} is measured as follows

$$C_{\text{stat}} = 5 \log \left(\frac{r_{80}}{r_{20}} \right), \quad (1)$$

where r_{80} and r_{20} are the radii containing 80% and 20% of the total flux respectively. The asymmetry parameter A_{stat} is measured by rotating the image by 180° , subtracting the rotated image from the original, and then normalizing by the total flux. This total image asymmetry is then reduced by the background component

$$A_{\text{stat}} = \frac{\sum_{ij} |I_{ij} - I_{ij}^{180}|}{\sum_{ij} |I_{ij}|} - B, \quad (2)$$

where I_{ij} and I_{ij}^{180} are the flux of a pixel in the original orientation and after rotating by 180° about the center of the galaxy, respectively. Here, B denotes the average asymmetry of the background. If we retain only valid STATMORPH measurements measured using SDSS images (by keeping data where both the asymmetry and concentration values are not None), this reduces the sample size to $n_{\text{stat}} = 520,331$. Similarly, by keeping valid STATMORPH measurements measured with UNIONS images, the sample size reduced to $n_{\text{stat,UNIONS}} = 198,626$.

We note that while there are other available morphological measurements, namely one measured by L. Simard et al. (2011), we use STATMORPH for the reason that it is applied homogeneously to both SDSS and UNIONS images.

2.2.2. Merger Classification

We complement traditional asymmetry-based merger identification methods with MUMMI (L. Ferreira et al. 2024, 2026). MUMMI employs a hybrid approach combining convolution neural networks and vision transformers, trained on realistic synthetic data from the illustrisTNG100-1 simulation (R. Weinberger et al. 2017; A. Pillepich et al. 2018). This framework enables highly accurate classification of merger stages achieving a purity rate of 95%. Crucially, due to its training data,

MUMMI is designed to identify mergers primarily in galaxies with stellar mass $M_* > 10^{10} M_\odot$ and covering mass ratio from 1:1 down to 1:10.

The catalog of mergers from UNIONS imaging is sourced from the published work by (L. Ferreira et al. 2024, 2026). To complement UNIONS with imaging at Dec < 30 deg, we also utilize a separate catalog of mergers identified by MUMMI applied to DECaLS imaging. This MUMMI-DECaLS catalog is currently unpublished and presented in Ellison et al. (in prep).

In both the UNIONS and DECaLS case, a galaxy’s merger status determined through a voting-based approach among different models. Specifically, we classify a galaxy as a merger if it receives the majority of votes in the ensemble classification process. After cross-matching with the SDSS catalog, a total of $n_{\text{MUMMI,UNIONS}} = 359,228$ and $n_{\text{MUMMI,DECaLS}} = 196,648$ galaxies from UNIONS and DECaLS have majority merger votes from MUMMI, as well as SDSS spectroscopic measurements.

2.3. TDE Host Galaxy Sample

We compiled our sample starting from the TDE catalogs in T. H. T. Wong et al. (2022), where the authors had already compiled a list of most likely TDE candidates from T. Wevers et al. (2017, 2019), K. D. French et al. (2020b), S. van Velzen et al. (2021), and S. Gezari (2021). We complement the list with recent discoveries from E. Hammerstein et al. (2023). For each TDE, we cross-matched its coordinate to the nearest galaxy within a 3-arcsecond radius using the SDSS DR7 spectroscopic catalog (M. A. Strauss et al. 2002) and UNIONS catalog, ensuring reliable host galaxy associations for subsequent analysis. Our sample includes eight galaxies that overlap with the J. Law-Smith et al. (2017) catalog ¹, supplemented by six newly identified TDE host galaxies, totaling 14 TDE host galaxies. Their RA and Dec. are presented in Table 1, and images are shown in Fig. 2.

The mass of the BH (M_{BH}) is a critical parameter in TDE physics, governing both the disruption radius of stars and the subsequent flare properties. We estimated M_{BH} through the $M_{\text{BH}} - \sigma$ relation (J. Kormendy & L. C. Ho 2013)

$$M_{\text{BH}} = 10^9 \times 0.309 \times (\sigma_e/200)^{4.38}, \quad (3)$$

prioritizing velocity dispersion (σ) measurements obtained from high-resolution Keck spectra (K. D. French

et al. 2016) for 10 out of 14 of our TDE host galaxies, and fall back to values from the MPA-JHU catalog (J. Brinchmann et al. 2004) when unavailable. All σ measurements from MPA-JHU were corrected to a standardized aperture using the relation from I. Jorgensen et al. (1995), accounting for variations in SDSS fiber sizes:

$$\sigma_e = \sigma_{v,\text{MPA}}/10^{-0.065 \times \log(r_e/1.5) - 0.013 \times \log^2(r_e/1.5)}, \quad (4)$$

where r_e is the effective radius from L. Simard et al. (2011). We acknowledge uncertainties in determining BH mass, stemming from various sources of σ and intrinsic scatter of the scaling relation (± 0.3 dex). Still, this hierarchical approach ensures consistent mass estimates across the TDE sample while prioritizing high-quality spectroscopic data when available.

2.4. Non-TDE Host Galaxy Control Sample

Key galaxy properties, such as stellar mass, correlate with M_{BH} and evolve with redshift (J. Kormendy & L. C. Ho 2013; S. Dattathri et al. 2025). A robust statistical comparison requires matching the TDE host sample to control galaxies with similar fundamental parameters. Therefore, we match our TDE host galaxies with galaxies of similar properties from SDSS. The following matching parameters are considered: redshift (z), black hole mass (M_{BH}), and total stellar mass of the host galaxy (M_*). First, we define a specific range for each matching parameter (± 0.1 dex for M_{BH} and M_* , and ± 0.01 for z) and randomly select a sample of $N = 500$ galaxies within these ranges. If the number of galaxies within these ranges is insufficient, we then relax our criteria and incrementally expand the range: by ± 0.05 dex for M_{BH} and M_* (up to a maximum of ± 0.25 dex), and by ± 0.005 for z (up to a maximum of ± 0.025). This process continues until the sample size reaches $N = 500$.

Subsequently, for each TDE host galaxy with morphological parameter X_{TDE} , we compare it with the corresponding measurement $X_{\text{control},j}$ from its control sample of 500 galaxies. Note that the control sample measurements were performed using the same survey as the matched TDE host galaxy. To account for the variations in match quality, we weight each control measurement following the method of D. R. Patton et al. (2016b). Specifically, a control galaxy at $z_{\text{control},j}$ within a redshift tolerance of $z_{\text{tol}} = 0.01$ of its matched TDE host galaxy at z_{TDE} will have a redshift weight of

$$w_{z,j} = 1 - \frac{|z_{\text{TDE}} - z_{\text{control},j}|}{z_{\text{tol}}}. \quad (5)$$

The overall weight is the product of the weights of all matching parameters:

$$w_j = w_{z,j} \cdot w_{M_{\text{BH}},j} \cdot w_{M_*,j}, \quad (6)$$

¹ TDE #9 in J. Law-Smith et al. (2017) is classified as a QSO, and TDE #10 has no optical spectra listed under any source in the SDSS. Hence, both are dropped from our sample.

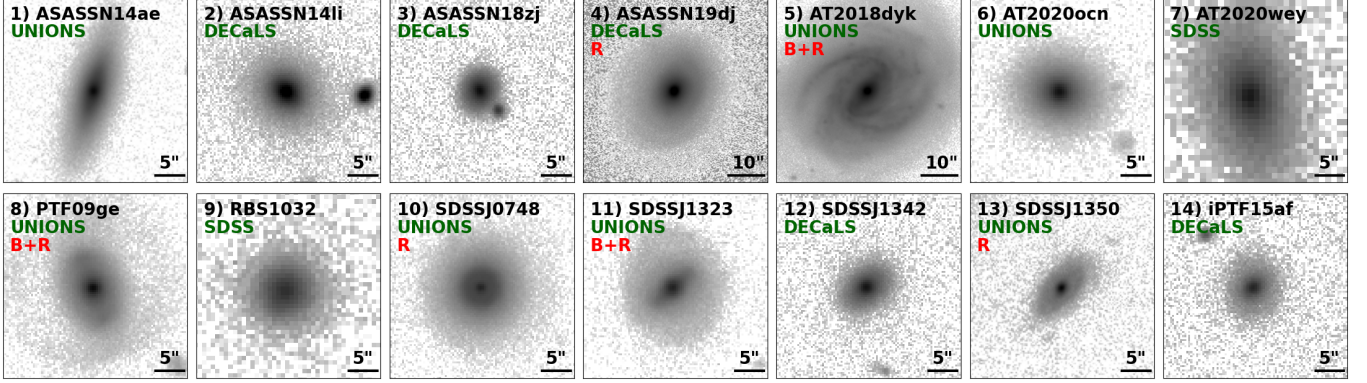


Figure 2. Representative r -band images of the 14 TDE host galaxies in Table 1. Images are sourced hierarchically: from UNIONS if available, otherwise from DECaLS, and finally from SDSS. Each panel indicates the TDE index, TDE name, its originating survey, and the structural classification (“R” for ring, and “B” for bar) in the top-left corner, with an angular size reference provided in the bottom-right corner.

i	TDE	RA [°]	DEC [°]	z	$\log(M_{\text{BH}}/M_{\odot})$	Type	reference
1	ASASSN-14ae*	167.167150	34.097845	0.043671	5.96	Optical/UV	K. D. French et al. (2020a)
2	ASASSN-14li	192.063457	17.774013	0.020648	6.77	X-ray	K. D. French et al. (2020a)
3	AT2018hyz (ASASSN-18zj)	151.711958	1.692786	0.045798	6.20	Optical/UV	K. D. French et al. (2020a)
4	AT2019azh (ASASSN-19dj)	123.320625	22.648302	0.022299	6.58	Optical/UV	E. Hammerstein et al. (2023)
5	AT2018dyk*	233.283416	44.535690	0.036753	7.39	Optical/UV	E. Hammerstein et al. (2023)
6	AT2020ocn*	208.474173	53.997150	0.070509	6.76	Optical/UV	E. Hammerstein et al. (2023)
7	AT2020wey	136.357788	61.802544	0.027413	5.56	Optical/UV	E. Hammerstein et al. (2023)
8	PTF09ge*	224.263268	49.611373	0.064706	6.79	Optical/UV	K. D. French et al. (2020a)
9	RBS1032	176.861244	49.716049	0.026087	5.81	X-ray	K. D. French et al. (2020a)
10	SDSSJ0748*	117.086119	47.203960	0.061533	7.61	Optical/UV	K. D. French et al. (2020a)
11	SDSSJ1323*	200.924890	48.450351	0.087540	6.62	X-ray	K. D. French et al. (2020a)
12	SDSSJ1342	205.685065	5.515594	0.036644	6.55	Optical/UV	K. D. French et al. (2020a)
13	SDSSJ1350*	207.506230	29.269355	0.077726	7.92	Optical/UV	K. D. French et al. (2020a)
14	iPTF15af	132.117261	22.059302	0.078997	7.28	Optical/UV	K. D. French et al. (2020a)

Table 1. Properties of the 14 TDEs. For each TDE, the table lists its index i , TDE name, RAs, Dec., redshift z , BH mass M_{BH} , TDE type, and reference. The 7 TDE host galaxies that are also found in UNIONS are highlighted with *. M_{BH} derived using σ from Keck are in bold; all other M_{BH} are derived using σ from the MPA-JHU catalog.

where $w_{M_{\text{BH}},j}$ and $w_{M_*,j}$ are the weights corresponding to the matching parameters M_{BH} and M_* . With these weights, we compute the weighted mean of the controls

$$\bar{X}_{\text{control}} = \frac{\sum_j w_j \cdot X_{\text{control},j}}{\sum_j w_j}. \quad (7)$$

We then compute the difference between the TDE host galaxies’ parameters and the weighted mean of its controls as:

$$\Delta X = X_{\text{TDE}} - \bar{X}_{\text{control}}. \quad (8)$$

We discuss how the uncertainties are obtained in Appendix B.

2.5. Identification of Ring and Bar Structures

Fig. 3 shows two examples of the TDE host galaxies in which we are able to obtain both SDSS (top), and DECaLS or UNIONS (bottom) images. This comparison demonstrates the improved image quality that DECaLS and UNIONS provides (resolution and depth). They reveals a wealth of morphological detail about TDE host galaxies that was previously inaccessible in SDSS data. Take **PTF09ge** as an example, its ring structure is particularly striking in the UNIONS image compared to that of the SDSS. It displays two bright nuclear patches surrounded by a faint outer ring, a configuration reminiscent of the R_1 or R'_1 morphology (characterized by a 180-degree winding of spiral arms that form a ring

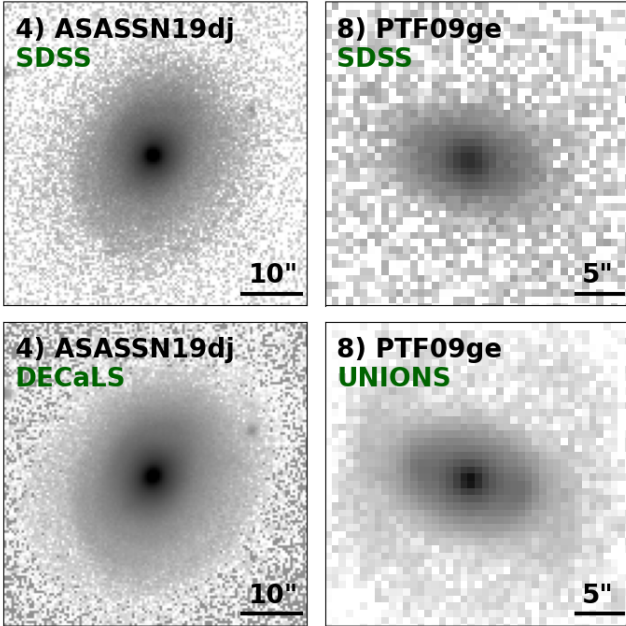


Figure 3. Comparison of r -band images for TDE host galaxies ASASSN-19dj (left) and PTF09ge (right) from different surveys. The top row display images from SDSS DR7, while the bottom row shows images from DECaLS (for ASASSN-19dj, bottom left) and UNIONS (for PTF09ge, bottom-right). The side-by-side comparison clearly demonstrates the significantly enhanced resolution of DECaLS and UNIONS imaging relative to SDSS. An angular size reference is provided in the bottom-right corner of each panel.

or pseudo-ring) in [R. J. Buta \(2017\)](#). This structure aligns with HST/WFC3 observations by [K. D. French et al. \(2020a\)](#), which confirmed both the blue outer ring and potential bar features of this particular galaxy. Another example is **ASASSN-19dj**, where faint ring-like or shell-like features are barely discernible in the SDSS image but appear significantly more prominent in DECaLS imagery.

We developed a systematic approach to classify the presence of bars and rings in our galaxy sample. Our analysis began with twelve TDE host galaxies with high-resolution imaging (seven identified in UNIONS and five in DECaLS). For each TDE host galaxy, JC compiled images of 10 randomly selected control galaxies from the same survey, drawing from the control samples established following [Sec. 2.4](#). NC subsequently randomly shuffled these images and provided them to CB, RKC and JD for independent, double-blinded visual classification, ensuring that the classifiers were unaware of which galaxies were TDE hosts. The vote assignments followed a three-tiered confidence system: confidence presence of the feature, uncertain presence of the feature, and no

detected feature. For the TDE host galaxies, we quantified the presence of features by assigning a score of 1 for confidently identified features and 0.5 for uncertain features, effectively weighting uncertain classifications accordingly. A TDE host galaxy was considered to possess a ring/bar if its averaged score was above 0.5. For the control galaxies, we determined the fraction with confidently identified features as a lower limit, and including uncertain classification as an upper limit, thus providing a range for the estimated feature prevalence.

We also obtain ring and bar fractions from citizen projects GALAXY CRUISE and Galaxy Zoo DESI. GALAXY CRUISE ([M. Tanaka et al. 2023](#)) is a citizen science project that contains morphological classification, which is based on the 2nd data release from the Hyper Suprime-Cam, Subaru Strategic Program (HSC-SSP) of 20,686 galaxies at $z < 0.2$. We cross-match this GALAXY CRUISE catalog with our SDSS catalog, finding 14,990 matches within 3". Unfortunately, our list of TDE host galaxies did not overlap with this cross-matched sample, meaning no GALAXY CRUISE classifications are available for them. We are interested in the 3rd question in the survey, where one can pick one out of four options (Ring, Fan, Tail, or Distorted) for the features of the galaxy. Following the classification criteria from [R. Shimakawa et al. \(2024\)](#), we consider the galaxy to be ringed if:

$$(P(\text{interact}) > 0.5) \cap (P(\text{ring}) = \max(P_i)), \quad (9)$$

and non-ring if

$$(P(\text{spiral}) < 0.5) \cap (P(\text{ring}) < \max(P_i)). \quad (10)$$

Here, $P(\text{spiral})$ and $P(\text{interact})$ give the probability of the galaxy showing spiral structures and evidence of interaction, based on Questions 1 and 2 respectively. $P_i \in \{P(\text{ring}), P(\text{fan}), P(\text{tail}), P(\text{distorted})\}$ represents the respective probabilities assigned in Question 3 that the galaxy exhibits each type of specific morphological disturbance. These individual probabilities satisfy the condition $\sum_i P_i = 1$.

On the other hand, we compute the bar fraction using morphology classification from [M. Walmsley et al. \(2023\)](#). These classifications are made using a deep learning model trained on Galaxy Zoo, containing votes for DESI Legacy Survey ([A. Dey et al. 2019](#)) DR8 and historical Galaxy Zoo DECaLS votes. We cross-match this result with the SDSS catalog and find 110,069 matches with a 3 arcsec matching tolerance, non of which overlaps with our list of TDE host galaxies. Regarding bar features, each galaxy has a predicted fraction of votes in three class: strong bar, weak bar, and no bar. We label each galaxy with the class with the

highest vote fraction, and consider the fraction of galaxies with strong bars to be a lower limit, and fraction of galaxies with strong or weak bar to be an upper limit of the predicted bar fraction.

2.6. Star-forming Main Sequence and Green Valley

The observed incidence of TDEs in the GV (J. Law-Smith et al. 2017; E. Hammerstein et al. 2021; Y. Yao et al. 2023) necessitates a precise operational definition to distinguish these transitional systems from both star-forming and quiescent populations. We base our GV definition on the star-forming main sequence (SFMS), the well-established correlation between M_* and SFR for star-forming galaxies (J. Brinchmann et al. 2004; K. G. Noeske et al. 2007). Following M. Donnari et al. (2019), we implement an iterative fitting procedure. We first bin galaxies into 0.2 dex intervals of M_* . For each mass bin, we iteratively calculate a clipped mean SFR and standard deviation σ , then linearly extrapolate the SFR– M_* relation until the SFR is affected by the quiescent region (where adjacent bins show $> 1\sigma$ deviation in mean SFR, typically cut at $\log M_* = 10.2$). After excluding outliers ($> 2\sigma$ below the trend), we repeat this process until achieving convergence (slope variation < 0.001 between iterations). The SFMS can be described by

$$\log(\text{SFR}) = 0.72 \log(M_*) - 7.03, \quad (11)$$

and the lower SFMS boundary is established at 1σ below this converged relation.

Within this framework, we define star-forming galaxies as those lying above the lower SFMS boundary, while the GV occupies the crucial transitional space starting from the lower SFMS boundary to 1 dex below it. This operational definition captures the GV’s evolutionary significance as the intermediate phase between blue, star-forming galaxies and red, quiescent systems (S. Salim 2014), while remaining consistent with established classification schemes (J. Law-Smith et al. 2017; S. A. Dodd et al. 2021). The resulting GV boundaries provide the necessary foundation for our subsequent analysis of TDE environments, and can be described by the following equation

$$0.83 \log(M_*) - 8.67 < \log(\text{SFR}) < 0.83 \log(M_*) - 7.67. \quad (12)$$

We refer to Sec. 3.5 for a visual of the boundaries.

3. RESULTS

3.1. General Properties of TDE Hosts

We compare our sample of 14 SDSS TDE host galaxies (Table 1) with the general SDSS galaxy population in Fig. 4. The gray contours show the general galaxy

distribution, while our TDE hosts are marked as red circles with their corresponding indices from Table 1. Our TDE hosts have BH masses $10^6 - 10^7 M_\odot$, consistent with T. Wevers et al. (2017), and relatively low stellar masses, following the expected $M_{\text{BH}} - M_*$ relation. Additionally, all TDEs in our sample have low redshifts ($z = 0.02 - 0.09$), reflecting current survey detection limits. Their star formation rates place them mostly in the GV between the star-forming main sequence and quiescent galaxies. Specifically, nine of the TDE hosts are located in the GV, three reside on the SFMS, and the remaining two are quiescent. Their bluer bulge colors ($B_g - B_r < 1$) indicate younger nuclear stellar populations. The TDE hosts display intermediate Sersic indices ($n \sim 2 - 4$), suggesting pseudo-bulges or disturbed morphologies, and span a wide range of bulge-to-total ratios (B/T). These trends (lower M_{BH} and M_* , bluer bulges, intermediate bulge structures, and GV SFRs) align closely with the findings of J. Law-Smith et al. (2017), reinforcing that TDEs preferentially occur in galaxies with recent central star formation and distinct nuclear properties.

3.2. Concentration of Stellar Density

Central stellar concentration has been shown to significantly relate to the rate of TDEs in galaxies (K. D. French et al. 2020b; H. Pfister et al. 2020; J. N. Y. Chang et al. 2025).

The top panel of Fig. 5 displays the STATMORPH concentration parameters C_{stat} of the TDE host galaxies (stars) and their control samples (crosses) in relation to M_{BH} , M_* , and z . Control sample measurements were weighted-averaged over 500 samples and obtained using the same survey as their matched TDE host, color-coded with yellow for UNIONS and blue for SDSS. Overall, C_{stat} increases steadily with M_{BH} and M_* , aligning with the expectation that concentration increases with total mass, reflecting the transition from disk-dominated to bulge-dominated systems in the mass sequence (X.-F. Deng 2013).

The bottom panel of Fig. 5 shows $\Delta C_{\text{stat}} = C_{\text{stat,TDE}} - \bar{C}_{\text{stat,control}}$ for each TDE. TDE hosts with UNIONS images are represented in blue, and others with SDSS images are represented in orange. Additionally, a histogram of the ΔC_{stat} distribution is provided on the right, with the shaded region indicating the average of ΔC_{stat} with a 1σ uncertainty. Details of the uncertainties are discussed in Appendix B.

One can see that ΔC_{stat} is consistently above 0. The mean value across all 14 TDE hosts is $\Delta C = 0.37 \pm 0.73$, indicating that TDE hosts are $\sim 16\%$ more concentrated than the control galaxy samples. When focus-

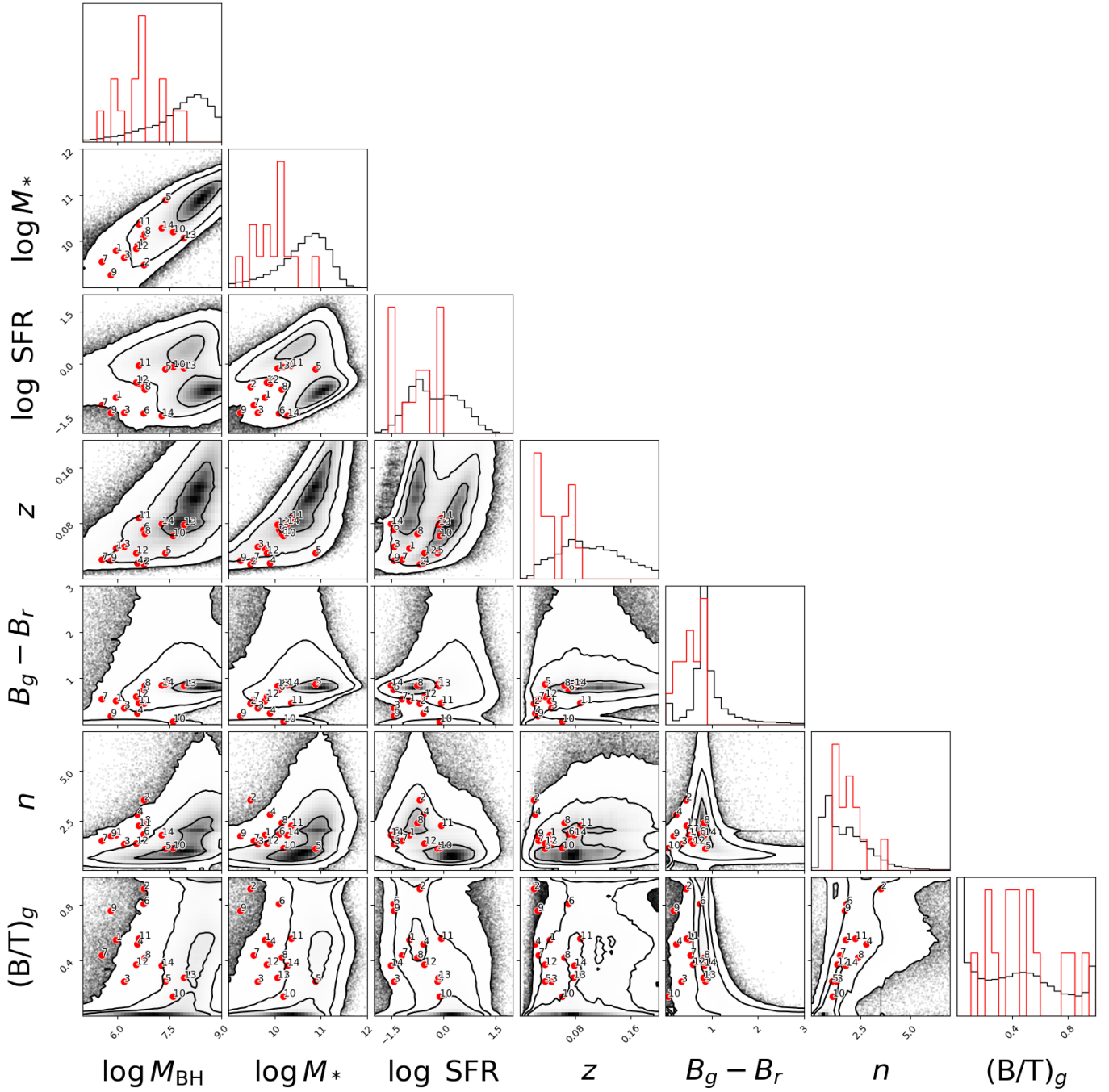


Figure 4. Corner plots comparing parameter distributions of the general SDSS galaxy population (contours) and our TDE host galaxy sample (red circles). Each red circle marker is annotated with its corresponding index from Table 1. The parameters displayed (from left to right) are: black hole mass M_{BH} , stellar mass M_* , star-formation rate SFR, redshift z , bulge color $B_g - B_r$, Sersic index n , and bulge-to-total ratio $(B/T)_g$. The contours represent the 1σ , 2σ , and 3σ confidence levels of the SDSS galaxy distribution. These plots reveal that TDE hosts tend to have lower black hole and stellar masses, reside at low redshifts, exhibit bluer bulge colors indicative of younger stellar populations, and possess intermediate structural properties such as Sersic index and bulge dominance.

ing solely on the UNIONS data, ΔC slightly increases to 0.37 ± 0.05 . Interestingly, high ΔC_{stat} TDE hosts are predominantly found in intermediate-mass systems, with no obvious trend observed with z . It is difficult to determine whether this observation is skewed by a few systems with particularly high C_{stat} , namely ASASSN-19dj and SDSSJ1350. Further data are needed to fully understand these trends.

3.3. Asymmetry of Galaxy Structure

The structure of a galaxy, especially its asymmetry, can provide important insight to its recent and ongoing merger activity (C. J. Conselice 2003; D. R. Patton et al. 2016a). In this section, we investigate the asymmetry of our TDE host galaxies compared to their control samples, to assess the role that mergers may play in their evolution.

The top panel of Fig. 6 plots the STATMORPH asymmetry parameter (A_{stat}) for the TDE host galaxies (star symbols) and their control samples (cross symbols) against M_{BH} , M_* , and z . As in Fig. 5, the measurements are color-coded by survey: blue for UNIONS and orange for SDSS. The bottom panel presents the difference in asymmetry, $\Delta A_{\text{stat}} = A_{\text{stat,TDE}} - A_{\text{stat,control}}$. The green shaded region denotes the mean ΔA_{stat} across all TDE hosts, while the histogram on the right shows the corresponding distribution of residuals.

Surprisingly, the results indicate no significant evidence of increased asymmetry in our TDE host galaxies. The averaged ΔA_{stat} across the sample is -0.02 ± 0.01 , suggesting that, on average, TDE hosts do not exhibit more asymmetric features than their control counterparts. Focusing on the UNIONS sample further lower ΔA_{stat} to -0.06 ± 0.02 .

Our results appear to suggest a negative correlation between ΔA_{stat} and M_* . However, closer examination reveals that this apparent relationship is primarily attributable to differences in image quality, as evidenced by clear separation of ΔA_{stat} estimates for SDSS and UNIONS hosts. Improving image quality generally reveals more faint asymmetric structures in galaxies, but preferentially in galaxies that are intrinsically asymmetric (C. Bottrell et al. 2019; M. D. Thorp et al. 2021; S. Wilkinson et al. 2024). Upper panels of Fig. 6 show that UNIONS controls are more asymmetric than SDSS controls, while TDE host asymmetries are less distinct between SDSS and improved UNIONS imaging. These preferentially boosted control asymmetries in UNIONS result in suppressed average ΔA_{stat} for UNIONS TDE hosts relative to SDSS. TDE hosts with UNIONS imaging coincidentally have higher stellar masses and are found at higher redshifts, resulting in an apparent trend.

If we had UNIONS images for all TDE hosts, we could potentially eliminate this apparent correlation.

We perform a similar analysis using asymmetry measurements from L. Simard et al. (2011) in Appendix C. TDE host galaxies are not enhanced in this asymmetry measurement either. To robustly characterize the morphological features of TDE hosts, future studies should incorporate images from combined surveys and develop a systematic approach to measuring these morphological measurements across surveys (e.g. E. Sazonova et al. 2024).

3.4. Post-merger Classification

Another way to assess whether these TDE host galaxies have likely undergone recent galaxy mergers is to use UNIONS’ MUMMI (L. Ferreira et al. 2024, 2026). In the MUMMI catalog, each galaxy is classified using 20 independently trained models to determine whether it is a merger. The galaxy’s merger status is then assigned based on the number of models that vote it as a merger. For our analysis, a galaxy is classified as a merger if more than 10 out of the 20 models vote it as such. This criterion is applied consistently to both TDE host galaxies and the control samples.

Among the 12 TDE host galaxies that are covered by MUMMI, all were classified as non-mergers. In contrast, 4.9% of the UNIONS controls and 5.2% of the DECaLS controls were identified as mergers. When combining both datasets, the overall merger fraction among the controls is approximately 5.03%, whereas none of the TDE hosts are classified as mergers.

Given the small sample size and the low expected merger rate ($\sim 5\%$ from the controls), we acknowledge the statistical uncertainty inherent in these estimates. To quantify this, we employ a Bayesian approach, with a prior merger rate of 5% modeled using a beta distribution $\beta(\alpha_{\text{prior}} = 1, \beta_{\text{prior}} = 19)$. For the TDE hosts, the number of “successes” (0 mergers out of 12 galaxies) can be modeled with a binomial likelihood. Combining the prior with the likelihood gives a posterior of $\beta(\alpha_{\text{posterior}}, \beta_{\text{posterior}} + 12)$. This approach indicates that the true merger rate is around 3.1%, with a 95% highest density interval of 0.1% – 9.2%.

Both the findings from image morphology analysis and MUMMI classification suggest that our TDE host galaxies do not exhibit enhanced merger activity compared to their controls. The heightened concentration in TDE hosts without a matching increase in asymmetry raises questions about the underlying processes. Absence of expected asymmetrical features suggests recent merger-driven, nuclear burst of star formation are un-

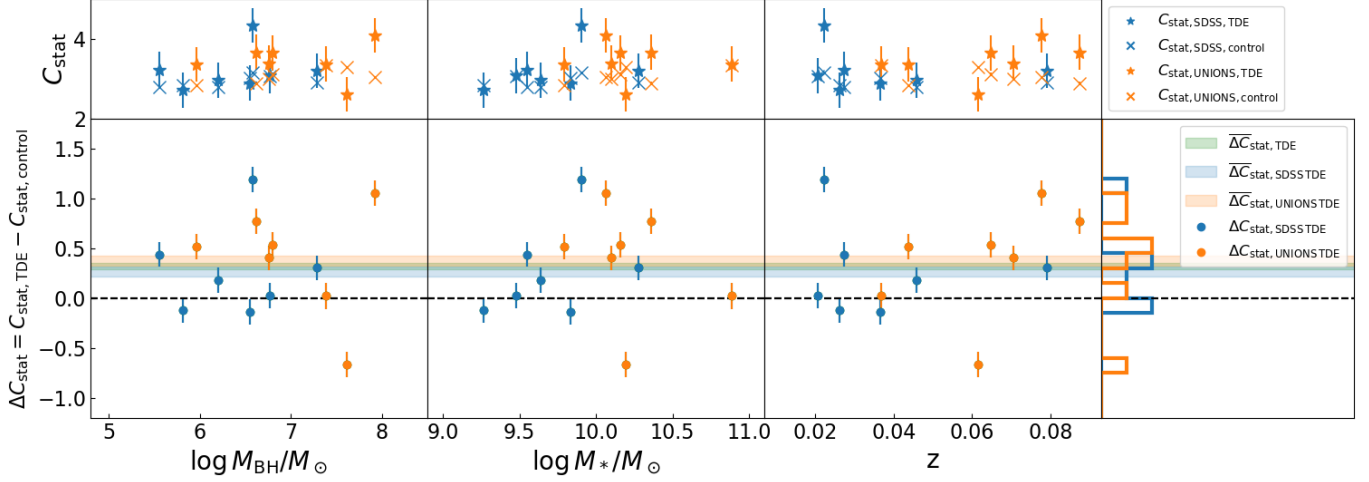


Figure 5. Concentration parameter analysis for TDE host galaxies and their control samples. The top panel presents the STATMORPH concentration parameter C_{stat} for TDE host galaxies (star symbol) and their control sample (cross symbol) as a function of M_{BH} , M_* , and z . Measurements are based on UNIONS images (orange) when available, and SDSS images (blue) otherwise. Importantly, the control sample measurements were weighted-averaged over 500 samples and consistently derived from the same survey as their TDE host galaxy. **The bottom panel displays the difference in concentration, $\Delta C_{\text{stat}} = C_{\text{stat},\text{TDE}} - \bar{C}_{\text{stat},\text{control}}$, with 1σ error bar.** The shaded region indicate the mean ΔC_{stat} for the UNIONS (orange), SDSS (blue), and combined (green) subsets. A dashed line marks $\Delta C_{\text{stat}} = 0$. The rightmost panel provides a histogram of ΔC for these different samples. **Overall, these results demonstrate that TDE host galaxies exhibit a significantly higher concentration parameter compared to their control samples, with an average $\Delta C_{\text{stat}} = 0.32 \pm 0.03$, implying TDE host galaxies are $\sim 16\%$ more concentrated.**

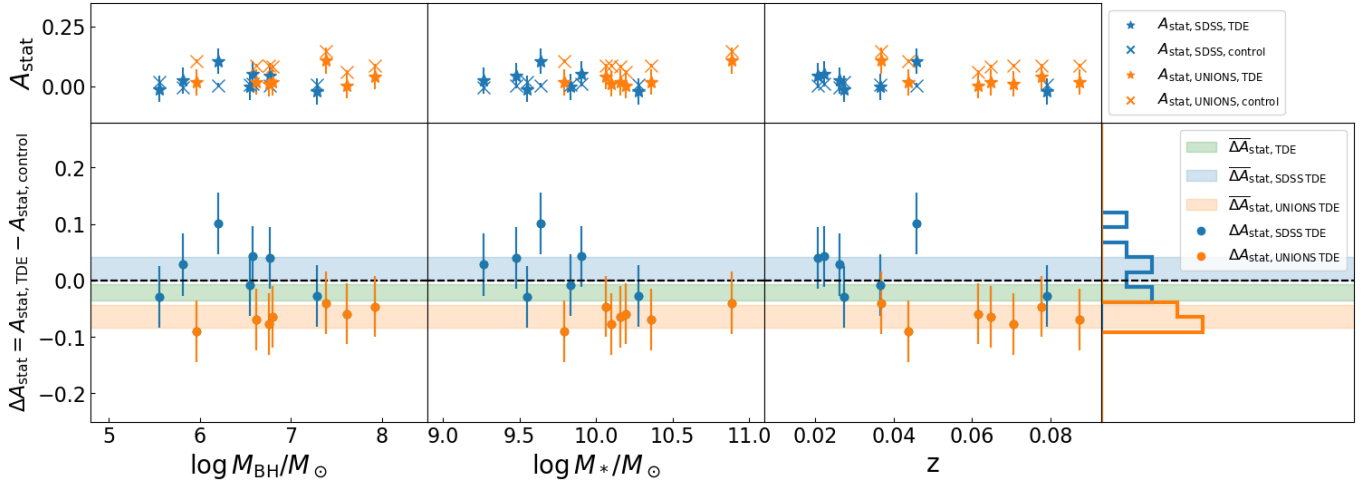


Figure 6. Asymmetry parameter analysis for TDE host galaxies and their control samples. The top panel presents the STATMORPH asymmetry parameter A_{stat} for TDE host galaxies (star symbol) and their control sample (cross symbol) as a function of M_{BH} , M_* , and z . As in Fig. 5, measurements are based on UNIONS images (orange symbol) when available, and SDSS images (blue symbols) otherwise. Control sample measurements were weighted-averaged over 500 samples and consistently derived from the same survey as their TDE host galaxy. **The bottom panel displays the difference in asymmetry parameter $\Delta A_{\text{stat}} = A_{\text{stat},\text{TDE}} - A_{\text{stat},\text{control}}$, with 1σ error bars.** The shaded regions indicate the mean ΔA_{stat} for the UNIONS (orange), SDSS (blue), and combined (green) subsets. A dashed line marks $\Delta A_{\text{stat}} = 0$. The rightmost panel provides a histogram of the ΔA_{stat} distribution for these different samples. **Overall, these results shows that TDE host galaxies, especially the higher-resolution UNIONS sample, shows no indication of enhanced asymmetry (and actually slightly reduced asymmetry) compared to their control sample.**

likely. Additionally, the MUMMI merger classifications do not support recent mergers or ongoing interactions in TDE hosts. Therefore, alternative mechanisms must be explored to understand how galaxies enhance their nuclear stellar concentration.

3.5. Bar and Ring Fraction

In this section, we investigate the bar and ring structures in TDE host galaxies and compare that with their control galaxies. Following the method mentioned in Sec. 2.5, we identify three TDE hosts with bar-like structures, and six TDE hosts with ring-like structures among the twelve TDE host galaxies that have quality imaging. Among the seven TDE hosts in the GV, three display bar-like structures and four display ring-like structures. We show the location of the TDE hosts in the SFR vs. M_* plot along with their classification in Fig. 7. As for the control samples, 13.6% – 20.0% of the galaxies display bar-like structures (lower limit set by confidently identified bar structures, and upper limit set by including uncertain bar identifications). At the same time, 16.9% – 24.0% of the controls displayed ring-like structures. When limited to the controls of GV TDEs, this barred fraction shifted slightly to 11.9% – 18.0%, and the ringed fraction shifted to 15.2% – 23.0%.

We compute reference ring and bar fractions from citizen projects GALAXY CRUISE and Galaxy Zoo DESI, respectively. These fractions are calculated from control samples matched in M_{BH} , M_* , and z to the TDE hosts, as described in Sec. 2.4). For controls matched to our full list of 14 TDE host sample, the ring fraction ranges from 10% – 35%, while for controls matched specifically to GV TDE hosts, it ranges from 11% – 39%. Similarly, the bar fraction ranges from 8% – 34% for all controls, increasing to 10% – 39% for the GV TDE host controls.

The ring and bar fractions derived from citizen projects exhibit a broader range than those from our own visual inspection. Our internal classifications lie predominantly in the lower part of these ranges, suggesting that our criteria are somewhat more conservative. However, because the classification process was conducted in a double-blinded manner, any systematic differences in classification strictness should affect both samples similarly. We therefore expect that the relative difference in ring and bar fraction between TDE hosts and controls remains robust.

Fig. 8 summarizes our findings on bar and ring fractions, revealing a significant enhancement of these structures in TDE host galaxies compared to their control counterparts. Specifically, the TDE host galaxy sample exhibits a bar fraction of 25%, representing a substantial 48% increase over the control sample’s average

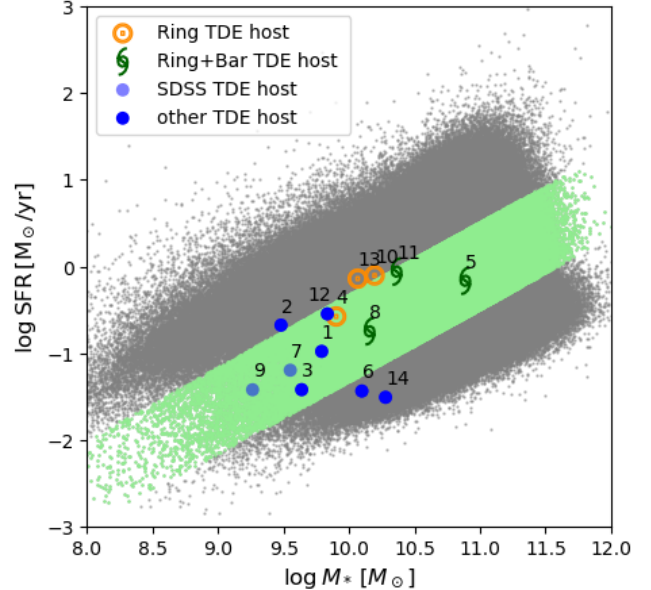


Figure 7. Location of 14 TDE host galaxies in the SFR vs. M_* plane. Different symbols represent the morphological classification (see Sec. 2.5) of the TDE host galaxies. The opacity of the symbols indicates the image resolution used for classification: more opaque symbols correspond to hosts with DECaLS or UNIONS images, while more transparent symbols denote hosts for which only SDSS images were available. The GV region, as defined in Eqn. 12, is shaded in green, with other regions shown in gray. **Notably, among the TDE host galaxies within the GV and observed with high-resolution imaging, three out of seven exhibit bar structures, and four out of seven display ring structures.**

bar fraction of 16.8% (averaged over upper and lower limit). Similarly, the TDE host galaxies show a ring fraction of 49%, which is a remarkable 144% increase compared to the control sample’s average ring fraction of 20.0%. This enhancement becomes even more pronounced when focusing on galaxies within the GV. In this transitional region, the TDE bar fraction soars to 42.9%, marking an impressive 187% increase relative to the GV control galaxies’ average bar fraction of 15.0%. Similarly, the GV TDE ring fraction is 57%, indicating a 200% increase over the GV control sample’s average ring fraction of 19.1%. These statistics underscore the strong correlation between these internal morphological features and TDE activity, particularly within the GV. **Overall, our sample of TDE host galaxies shows enhancement in bar and ring structures when compared to their control galaxies. This enhancement is more pronounced when focusing on galaxies in the GV.**

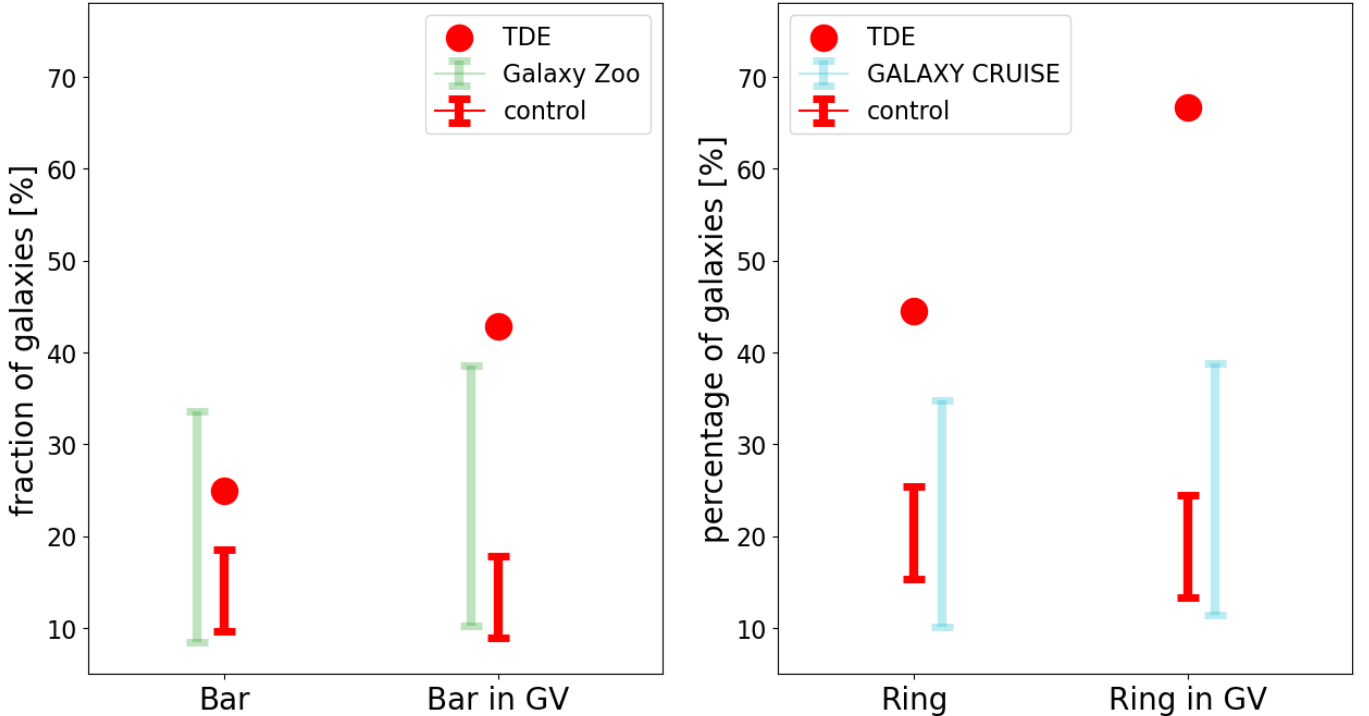


Figure 8. Bar (left panel) and ring (right panel) fractions for TDE host galaxies and various control samples. The bar/ring fraction for out TDE host galaxy sample, determined through visual classification, is indicated by red circles. Red bars represents the corresponding fraction for their matched control samples, classified using the identical visual method. These are shown for both the overall galaxy population and specifically for those within the GV. For comparison, bar and ring fractions from Galaxy Zoo (light green) and GALAXY CRUISE (light blue) control samples are also displayed. **Overall, these result indicate that TDE host galaxies are more likely to possess bar or ring structures than their control samples, with this enhancement being more pronounced among TDE hosts located in the GV.**

4. DISCUSSION

While our TDE host galaxies exhibit no enhanced merger activity compared to their controls, we find that a significant proportion of TDE host galaxies in our sample display bar-like and ring-like structures. This suggests that secular processes could be an alternative driver for the connection between the post-starburst status and enhanced central stellar concentrations of TDE host galaxies.

It is important to acknowledge potential observational biases that may influence these results. Many of the non-barrred or seemingly featureless galaxies in our sample could, in fact, host undetected structural features. Recent high-resolution studies with James Webb Space Telescope (JWST) have revealed that certain morphological structures can be missed or unresolved in lower-resolution surveys (V. Kuhn et al. 2024; Z. A. Le Conte et al. 2026a,b). Moreover, our own findings show that some TDE hosts classified as compact or featureless in SDSS images exhibit prominent bars or rings when observed with deeper, higher-resolution data from UNIONS or DeCaLS. This suggests that current survey sensitivities impose a lower limit on our ability to detect

such features, and the true fraction of barred and ringed galaxies may be underestimated. While advanced techniques such as generative forward modeling can be employed to recover morphological structures that are otherwise obscured or unresolved in lower-quality data (e.g. A. Adam et al. 2025), such methods were beyond the scope of our current analysis. Instead, we endeavored to mitigate these observational biases by carefully constructing unbiased control samples for our TDE hosts, matching them on z , M_{BH} , M_* , and critically, imaging quality.

Nevertheless, for the TDE hosts in which bar or ring features are present, secular evolution driven by bars provides a compelling physical framework. Secular evolution, characterized by gradual internal changes in relatively isolated galaxies, plays a critical role in shaping galactic nuclei. Bars, in particular, generate non-axisymmetric gravitational potentials that torque gas toward the center (E. Athanassoula 1992; B. G. Piner et al. 1995; P. Englmaier & O. Gerhard 1997), producing radial shocks and resonant interactions that drive material inward (W. W. Roberts et al. 1979; P. Verwilghen et al. 2024). Critically, resonance interactions between

the bar and gas not only drive central inflows but also concentrate material into rings (R. J. Buta 2017; M. C. Sormani et al. 2018). Recent work by M. Frosst et al. (2025) further supports this picture, demonstrating that barred galaxies host more massive central BHs than unbarred controls, likely due to the efficiency of bar-driven gas inflow in fueling both star formation and BH growth.

As bars funnel gas inward, they trigger nuclear starbursts (C. H. Heller & I. Shlosman 1994; W. W. Roberts et al. 1979; J. Kormendy & R. C. Kennicutt 2004; R. J. Buta 2017; S. L. Ellison et al. 2011). Whether this inflow also efficiently feeds AGN remains an open question. While some studies find a correlation between bars and AGN activities (L. C. Ho 2005; S. Alonso et al. 2018), others report no significant connection (M. A. Galloway et al. 2015; A. D. Goulding et al. 2017).

The stellar feedback from the triggered nuclear starburst (e.g. supernova, winds) may subsequently deplete and/or heat gas reservoirs (C. C. Hayward & P. F. Hopkins 2017; H. He et al. 2023), while AGN feedback may further reduce the availability of star-forming gas (J. R. Mullane et al. 2015; T. T. Shimizu et al. 2015). Notably, the structure of the bars also influence star formation in complex ways: shear forces in dust lanes can suppress massive star formation, while shocks enhance it (A. Zurita et al. 2004). Collectively, these mechanisms can leave post-starburst signatures in galaxies.

Thus, secular evolution driven by large-scale bars provides a compelling framework to explain several observed properties of TDE host galaxies. Bars can funnel gas inward to enhance central stellar densities and trigger nuclear starbursts (and potentially accelerate AGN activity), resulting in post-starburst galaxies. Crucially, this process increases central stellar concentration without inducing significant global asymmetry, aligning with our findings. Furthermore, bars can dynamically enhance TDE rates: stars trapped in bar-aligned orbits can develop high eccentricities (E. Athanassoula 1992), and subsequent perturbations could efficiently scatter these stars into the loss cone where they will eventually be disrupted (D. Merritt & M. Y. Poon 2004).

However, bars alone may not be the sole mechanism responsible for the formation of a dense nuclear stellar distribution and subsequent TDE events. Bars are correlated with stellar mass and galaxy morphology, being more prominent in massive, late-type spiral galaxies, while weaker bars are observed in low-mass early-type dwarfs and irregular galaxies (P. Erwin 2018). Despite this correlation, TDEs have been observed in low-mass galaxies, necessitating further investigation to enhance our current understanding.

5. SUMMARY

In this study, we examined the morphology and physical properties of TDE host galaxies based on imaging data from SDSS, DECaLS and UNIONS. From a reference catalog of known TDE events, we identified 14 matching host galaxies from the SDSS spectroscopic sample. We compared host properties to matched, non-TDE hosting controls in redshifts, stellar mass, and black hole mass. We compare the morphologies of TDE host galaxies to their controls using visual classifications, structural measurements, and a machine learning-based merger classifier. We provide a summary of our findings below.

- TDE host galaxies exhibit a notable increase in concentration compared to their control sample ($\Delta C_{\text{stat}} = 0.32 \pm 0.03$), indicating they are $\sim 16\%$ more concentrated. This suggests an enhancement in central stellar density near the MBH.
- Our analysis of TDE host galaxies reveals a lack of enhancement in asymmetry in comparison to their control sample, with $\Delta A_{\text{stat}} = -0.02 \pm 0.01$. Additionally, there are no indications that these TDE hosts are recent merger remnants or currently undergoing interactions, based on merger classifications from the machine-learning model MUMMI. This surprising result does not favor the merger-driven origin of TDE hosts.
- TDE host galaxies show enhanced bar-like and ring-like structures. Notably, among green valley galaxies, this enhancement is almost tripled compared to their controls. This suggests that bar-driven secular evolution may play a key role in funneling gas toward the galaxy center, thereby increasing central stellar density and potentially triggering TDEs.

Our findings offer valuable insights into TDE host galaxy environments, underscoring the importance of studying their morphological and structural features. The observed increase in concentration and the prevalence of bar-like and ring-like structures suggest that internal, secular process, such as bar-driven gas inflow, plays a crucial role in the evolution of TDE host galaxies in the low- z universe. While both galaxy mergers and bars are known to enhance star formation, our results point to a distinct mechanism for TDE triggering. The relative absence of prominent recent merger signatures in our sample, coupled with these internal features, challenges the previous assumption that external galaxy interaction is the main TDE triggers.

Still, our current understanding is limited by sample size; only a small fraction of ~ 100 observed TDEs have

imaging suitable for our morphological analysis. Expanding this analysis with larger, uniformly characterized datasets is essential for confirming these trends and deepening our understanding of the physical processes underlying TDEs. Future deep, high-resolution and high-cadence imaging from next-generation facilities like the Vera C. Rubin Observatory will be crucial (Ž. Ivezić et al. 2019; F. B. Bianco et al. 2022) alongside complementary spectroscopic campaigns. Rubin is expected to identify ~ 1000 TDEs per year (S. van Velzen et al. 2019; K. Bricman & A. Gomboc 2020) and simultaneously produce high-quality imaging for their hosts. Furthermore, Rubin’s depth will extend TDE host galaxy samples to higher redshifts where galaxy mergers are more frequent. This will be critical for disentangling the relative contributions of internal (secular) and external (merger-driven) processes to TDE rates across cosmic time.

ACKNOWLEDGMENTS

We thank I. Arcavi, K. Auchettl, S. Dodd, I. Ebrova, I. Mendel, and E. Ramirez-Ruiz for useful comments and discussions. We thank the participants of the TDE FORUM (Full-process Orbital to Radiative Unified Modeling) online seminar series for their inspiring discussions. We are also grateful to NC for their help in the visual classification process. JC, LD and RKC acknowledge support from the National Natural Science Foundation of China and the Hong Kong Research Grants Council (NSFC/RGC JRS N_HKU782/23, RGC GRF 17314822). RKC would like to acknowledge the financial support provided by the Anusandhan National Research Foundation (ANRF), a statutory body of the Department of Science and Technology (DST), Govern-

ment of India, through the National Post-Doctoral Fellowship (NPDF) [Grant No. PDF/2025/004682]. CB gratefully acknowledges support from the Forrest Research Foundation. RY acknowledges support by National Natural Science Foundation of China (grant No. 12425302 and 12373008), by Research Grant Council of Hong Kong (GRF 14303123), by Jockey Club Charities Trust through the JC STEM Lab of Astronomical Instrumentation, and by CUHK Direct Grant.

We are honored and grateful for the opportunity to observe the Universe from Maunakea and Haleakala, which both have cultural, historical and natural significance in Hawaii. This work is based on data obtained as part of the Canada-France Imaging Survey, a CFHT large program of the National Research Council of Canada and the French Centre National de la Recherche Scientifique. Based on observations obtained with MegaPrime/MegaCam, a joint project of CFHT and CEA Saclay, at the Canada-France-Hawaii Telescope (CFHT) which is operated by the National Research Council (NRC) of Canada, the Institut National des Science de l’Univers (INSU) of the Centre National de la Recherche Scientifique (CNRS) of France, and the University of Hawaii. This research used the facilities of the Canadian Astronomy Data Centre operated by the National Research Council of Canada with the support of the Canadian Space Agency. This research is based in part on data collected at Subaru Telescope, which is operated by the National Astronomical Observatory of Japan. Pan-STARRS is a project of the Institute for Astronomy of the University of Hawaii, and is supported by the NASA SSO Near Earth Observation Program under grants 80NSSC18K0971, NNX14AM74G, NNX12AR65G, NNX13AQ47G, NNX08AR22G, 80NSSC21K1572 and by the State of Hawaii.

REFERENCES

- Abazajian, K. N., Adelman-McCarthy, J. K., Agüeros, M. A., et al. 2009, *ApJS*, 182, 543, doi: [10.1088/0067-0049/182/2/543](https://doi.org/10.1088/0067-0049/182/2/543)
- Adam, A., Stone, C., Bottrell, C., et al. 2025, *AJ*, 169, 254, doi: [10.3847/1538-3881/adb039](https://doi.org/10.3847/1538-3881/adb039)
- Alonso, S., Coldwell, G., Duplancic, F., Mesa, V., & Lambas, D. G. 2018, *A&A*, 618, A149, doi: [10.1051/0004-6361/201832796](https://doi.org/10.1051/0004-6361/201832796)
- Athanassoula, E. 1992, *MNRAS*, 259, 328, doi: [10.1093/mnras/259.2.328](https://doi.org/10.1093/mnras/259.2.328)
- Barnes, J. E., & Hernquist, L. 1998, *ApJ*, 495, 187, doi: [10.1086/305294](https://doi.org/10.1086/305294)
- Bianco, F. B., Ivezić, Ž., Jones, R. L., et al. 2022, *ApJS*, 258, 1, doi: [10.3847/1538-4365/ac3e72](https://doi.org/10.3847/1538-4365/ac3e72)
- Bickley, R. W., Bottrell, C., Hani, M. H., et al. 2021, *MNRAS*, 504, 372, doi: [10.1093/mnras/stab806](https://doi.org/10.1093/mnras/stab806)
- Blum, R. D., Burleigh, K., Dey, A., et al. 2016, in *American Astronomical Society Meeting Abstracts*, Vol. 228, American Astronomical Society Meeting Abstracts #228, 317.01
- Bonnerot, C., & Stone, N. C. 2021, *SSRv*, 217, 16, doi: [10.1007/s11214-020-00789-1](https://doi.org/10.1007/s11214-020-00789-1)
- Bottrell, C., Simard, L., Mendel, J. T., & Ellison, S. L. 2019, *MNRAS*, 486, 390, doi: [10.1093/mnras/stz855](https://doi.org/10.1093/mnras/stz855)

- Bricman, K., & Gomboc, A. 2018, arXiv e-prints, arXiv:1812.06054, doi: [10.48550/arXiv.1812.06054](https://doi.org/10.48550/arXiv.1812.06054)
- Bricman, K., & Gomboc, A. 2020, *ApJ*, 890, 73, doi: [10.3847/1538-4357/ab6989](https://doi.org/10.3847/1538-4357/ab6989)
- Brinchmann, J., Charlot, S., White, S. D. M., et al. 2004, *MNRAS*, 351, 1151, doi: [10.1111/j.1365-2966.2004.07881.x](https://doi.org/10.1111/j.1365-2966.2004.07881.x)
- Brooks, A., & Christensen, C. 2016, in *Astrophysics and Space Science Library*, Vol. 418, Galactic Bulges, ed. E. Laurikainen, R. Peletier, & D. Gadotti, 317, doi: [10.1007/978-3-319-19378-6_12](https://doi.org/10.1007/978-3-319-19378-6_12)
- Buta, R. J. 2017, *MNRAS*, 471, 4027, doi: [10.1093/mnras/stx1829](https://doi.org/10.1093/mnras/stx1829)
- Byrne-Mamahit, S., Hani, M. H., Ellison, S. L., Quai, S., & Patton, D. R. 2023, *MNRAS*, 519, 4966, doi: [10.1093/mnras/stac3674](https://doi.org/10.1093/mnras/stac3674)
- Byrne-Mamahit, S., Patton, D. R., Ellison, S. L., et al. 2024, *MNRAS*, 528, 5864, doi: [10.1093/mnras/stae419](https://doi.org/10.1093/mnras/stae419)
- Chang, J. N. Y., Dai, L., Pfister, H., Kar Chowdhury, R., & Natarajan, P. 2025, *ApJL*, 980, L22, doi: [10.3847/2041-8213/adace7](https://doi.org/10.3847/2041-8213/adace7)
- Conselice, C. J. 2003, *ApJS*, 147, 1, doi: [10.1086/375001](https://doi.org/10.1086/375001)
- Dai, J. L., Lodato, G., & Cheng, R. 2021, *SSRv*, 217, 12, doi: [10.1007/s11214-020-00747-x](https://doi.org/10.1007/s11214-020-00747-x)
- Dattathri, S., Natarajan, P., Porras-Valverde, A. J., et al. 2025, *ApJ*, 984, 122, doi: [10.3847/1538-4357/adbeef](https://doi.org/10.3847/1538-4357/adbeef)
- Davis, T. A., van de Voort, F., Rowlands, K., et al. 2019, *MNRAS*, 484, 2447, doi: [10.1093/mnras/stz180](https://doi.org/10.1093/mnras/stz180)
- De Propriis, R., Conselice, C. J., Liske, J., et al. 2007, *ApJ*, 666, 212, doi: [10.1086/520488](https://doi.org/10.1086/520488)
- Deng, X.-F. 2013, *Research in Astronomy and Astrophysics*, 13, 651, doi: [10.1088/1674-4527/13/6/004](https://doi.org/10.1088/1674-4527/13/6/004)
- Dey, A., Schlegel, D. J., Lang, D., et al. 2019, *AJ*, 157, 168, doi: [10.3847/1538-3881/ab089d](https://doi.org/10.3847/1538-3881/ab089d)
- Dodd, S. A., Law-Smith, J. A. P., Auchettl, K., Ramirez-Ruiz, E., & Foley, R. J. 2021, *ApJL*, 907, L21, doi: [10.3847/2041-8213/abd852](https://doi.org/10.3847/2041-8213/abd852)
- Donnari, M., Pillepich, A., Nelson, D., et al. 2019, *MNRAS*, 485, 4817, doi: [10.1093/mnras/stz712](https://doi.org/10.1093/mnras/stz712)
- Ellison, S., Ferreira, L., Wild, V., et al. 2024, *The Open Journal of Astrophysics*, 7, 121, doi: [10.33232/001c.127779](https://doi.org/10.33232/001c.127779)
- Ellison, S. L., & Ferreira, L. 2025, arXiv e-prints, arXiv:2511.21512, doi: [10.48550/arXiv.2511.21512](https://doi.org/10.48550/arXiv.2511.21512)
- Ellison, S. L., Nair, P., Patton, D. R., et al. 2011, *MNRAS*, 416, 2182, doi: [10.1111/j.1365-2966.2011.19195.x](https://doi.org/10.1111/j.1365-2966.2011.19195.x)
- Ellison, S. L., Wilkinson, S., Woo, J., et al. 2022, *MNRAS*, 517, L92, doi: [10.1093/mnrasl/slac109](https://doi.org/10.1093/mnrasl/slac109)
- Englmaier, P., & Gerhard, O. 1997, *MNRAS*, 287, 57, doi: [10.1093/mnras/287.1.57](https://doi.org/10.1093/mnras/287.1.57)
- Erwin, P. 2018, *MNRAS*, 474, 5372, doi: [10.1093/mnras/stx3117](https://doi.org/10.1093/mnras/stx3117)
- Evans, C. R., & Kochanek, C. S. 1989, *ApJL*, 346, L13, doi: [10.1086/185567](https://doi.org/10.1086/185567)
- Ferreira, L., Ellison, S. L., Patton, D. R., et al. 2025, *MNRAS*, 538, L31, doi: [10.1093/mnrasl/slaf004](https://doi.org/10.1093/mnrasl/slaf004)
- Ferreira, L., Ellison, S. L., Patton, D. R., et al. 2026, arXiv e-prints, arXiv:2601.07604, doi: [10.48550/arXiv.2601.07604](https://doi.org/10.48550/arXiv.2601.07604)
- Ferreira, L., Bickley, R. W., Ellison, S. L., et al. 2024, *MNRAS*, 533, 2547, doi: [10.1093/mnras/stae1885](https://doi.org/10.1093/mnras/stae1885)
- French, K. D., Arcavi, I., & Zabludoff, A. 2016, *ApJL*, 818, L21, doi: [10.3847/2041-8205/818/1/L21](https://doi.org/10.3847/2041-8205/818/1/L21)
- French, K. D., Arcavi, I., Zabludoff, A. I., et al. 2020a, *ApJ*, 891, 93, doi: [10.3847/1538-4357/ab7450](https://doi.org/10.3847/1538-4357/ab7450)
- French, K. D., Wevers, T., Law-Smith, J., Graur, O., & Zabludoff, A. I. 2020b, *SSRv*, 216, 32, doi: [10.1007/s11214-020-00657-y](https://doi.org/10.1007/s11214-020-00657-y)
- Frosst, M., Obreschkow, D., Ludlow, A., Bottrell, C., & Genel, S. 2025, *MNRAS*, 537, 3543, doi: [10.1093/mnras/staf255](https://doi.org/10.1093/mnras/staf255)
- Galloway, M. A., Willett, K. W., Fortson, L. F., et al. 2015, *MNRAS*, 448, 3442, doi: [10.1093/mnras/stv235](https://doi.org/10.1093/mnras/stv235)
- Gezari, S. 2021, *ARA&A*, 59, 21, doi: [10.1146/annurev-astro-111720-030029](https://doi.org/10.1146/annurev-astro-111720-030029)
- Gezari, S., van Velzen, S., Hung, T., Cenko, B., & Arcavi, I. 2018, arXiv e-prints, arXiv:1812.07036, doi: [10.48550/arXiv.1812.07036](https://doi.org/10.48550/arXiv.1812.07036)
- Goulding, A. D., Matthaey, E., Greene, J. E., et al. 2017, *ApJ*, 843, 135, doi: [10.3847/1538-4357/aa755b](https://doi.org/10.3847/1538-4357/aa755b)
- Graur, O., French, K. D., Zahid, H. J., et al. 2018, *ApJ*, 853, 39, doi: [10.3847/1538-4357/aaa3fd](https://doi.org/10.3847/1538-4357/aaa3fd)
- Gwyn, S., McConnachie, A. W., Cuillandre, J.-C., et al. 2025, arXiv e-prints, arXiv:2503.13783, doi: [10.48550/arXiv.2503.13783](https://doi.org/10.48550/arXiv.2503.13783)
- Hammerstein, E., Gezari, S., van Velzen, S., et al. 2021, *ApJL*, 908, L20, doi: [10.3847/2041-8213/abdcb4](https://doi.org/10.3847/2041-8213/abdcb4)
- Hammerstein, E., van Velzen, S., Gezari, S., et al. 2023, *ApJ*, 942, 9, doi: [10.3847/1538-4357/aca283](https://doi.org/10.3847/1538-4357/aca283)
- Hayward, C. C., & Hopkins, P. F. 2017, *MNRAS*, 465, 1682, doi: [10.1093/mnras/stw2888](https://doi.org/10.1093/mnras/stw2888)
- He, H., Bottrell, C., Wilson, C., et al. 2023, *ApJ*, 950, 56, doi: [10.3847/1538-4357/acca76](https://doi.org/10.3847/1538-4357/acca76)
- Heller, C. H., & Shlosman, I. 1994, *ApJ*, 424, 84, doi: [10.1086/173874](https://doi.org/10.1086/173874)
- Hernquist, L. 1989, *Nature*, 340, 687, doi: [10.1038/340687a0](https://doi.org/10.1038/340687a0)
- Ho, L. C. 2005, *ApJ*, 629, 680, doi: [10.1086/431643](https://doi.org/10.1086/431643)
- Hopkins, P. F., Cox, T. J., Hernquist, L., et al. 2013, *MNRAS*, 430, 1901, doi: [10.1093/mnras/stt017](https://doi.org/10.1093/mnras/stt017)

- Ivezić, Ž., Kahn, S. M., Tyson, J. A., et al. 2019, *ApJ*, 873, 111, doi: [10.3847/1538-4357/ab042c](https://doi.org/10.3847/1538-4357/ab042c)
- Jorgensen, I., Franx, M., & Kjaergaard, P. 1995, *MNRAS*, 276, 1341, doi: [10.1093/mnras/276.4.1341](https://doi.org/10.1093/mnras/276.4.1341)
- Kormendy, J., & Ho, L. C. 2013, *ARA&A*, 51, 511, doi: [10.1146/annurev-astro-082708-101811](https://doi.org/10.1146/annurev-astro-082708-101811)
- Kormendy, J., & Kennicutt, Jr., R. C. 2004, *ARA&A*, 42, 603, doi: [10.1146/annurev.astro.42.053102.134024](https://doi.org/10.1146/annurev.astro.42.053102.134024)
- Kuhn, V., Guo, Y., Martin, A., et al. 2024, *ApJL*, 968, L15, doi: [10.3847/2041-8213/ad43eb](https://doi.org/10.3847/2041-8213/ad43eb)
- Law-Smith, J., Ramirez-Ruiz, E., Ellison, S. L., & Foley, R. J. 2017, *ApJ*, 850, 22, doi: [10.3847/1538-4357/aa94c7](https://doi.org/10.3847/1538-4357/aa94c7)
- Le Conte, Z. A., Gadotti, D. A., Harvey, T., et al. 2026a, arXiv e-prints, arXiv:2601.18871, doi: [10.48550/arXiv.2601.18871](https://doi.org/10.48550/arXiv.2601.18871)
- Le Conte, Z. A., Gadotti, D. A., Ferreira, L., et al. 2026b, *MNRAS*, 545, staf2010, doi: [10.1093/mnras/staf2010](https://doi.org/10.1093/mnras/staf2010)
- Lotz, J. M., Davis, M., Faber, S. M., et al. 2008, *ApJ*, 672, 177, doi: [10.1086/523659](https://doi.org/10.1086/523659)
- Lynden-Bell, D. 1967, *MNRAS*, 136, 101, doi: [10.1093/mnras/136.1.101](https://doi.org/10.1093/mnras/136.1.101)
- McElroy, R., Bottrell, C., Hani, M. H., et al. 2022, *MNRAS*, 515, 3406, doi: [10.1093/mnras/stac1715](https://doi.org/10.1093/mnras/stac1715)
- Mendel, J. T., Simard, L., Palmer, M., Ellison, S. L., & Patton, D. R. 2014, *ApJS*, 210, 3, doi: [10.1088/0067-0049/210/1/3](https://doi.org/10.1088/0067-0049/210/1/3)
- Merritt, D., & Poon, M. Y. 2004, *ApJ*, 606, 788, doi: [10.1086/382497](https://doi.org/10.1086/382497)
- Mullaney, J. R., Alexander, D. M., Aird, J., et al. 2015, *MNRAS*, 453, L83, doi: [10.1093/mnrasl/slv110](https://doi.org/10.1093/mnrasl/slv110)
- Noeske, K. G., Weiner, B. J., Faber, S. M., et al. 2007, *ApJL*, 660, L43, doi: [10.1086/517926](https://doi.org/10.1086/517926)
- Patton, D. R., Qamar, F. D., Ellison, S. L., et al. 2016a, *MNRAS*, 461, 2589, doi: [10.1093/mnras/stw1494](https://doi.org/10.1093/mnras/stw1494)
- Patton, D. R., Qamar, F. D., Ellison, S. L., et al. 2016b, *MNRAS*, 461, 2589, doi: [10.1093/mnras/stw1494](https://doi.org/10.1093/mnras/stw1494)
- Pawlik, M. M., McAlpine, S., Trayford, J. W., et al. 2019, *Nature Astronomy*, 3, 440, doi: [10.1038/s41550-019-0725-z](https://doi.org/10.1038/s41550-019-0725-z)
- Pfister, H., Bar-Or, B., Volonteri, M., Dubois, Y., & Capelo, P. R. 2019, *MNRAS*, 488, L29, doi: [10.1093/mnrasl/slz091](https://doi.org/10.1093/mnrasl/slz091)
- Pfister, H., Volonteri, M., Dai, J. L., & Colpi, M. 2020, *MNRAS*, 497, 2276, doi: [10.1093/mnras/staa1962](https://doi.org/10.1093/mnras/staa1962)
- Pillepich, A., Springel, V., Nelson, D., et al. 2018, *MNRAS*, 473, 4077, doi: [10.1093/mnras/stx2656](https://doi.org/10.1093/mnras/stx2656)
- Piner, B. G., Stone, J. M., & Teuben, P. J. 1995, *ApJ*, 449, 508, doi: [10.1086/176075](https://doi.org/10.1086/176075)
- Quai, S., Byrne-Mamahit, S., Ellison, S. L., Patton, D. R., & Hani, M. H. 2023, *MNRAS*, 519, 2119, doi: [10.1093/mnras/stac3713](https://doi.org/10.1093/mnras/stac3713)
- Rees, M. J. 1988, *Nature*, 333, 523, doi: [10.1038/333523a0](https://doi.org/10.1038/333523a0)
- Renaud, F., Segovia Otero, Á., & Agertz, O. 2022, *MNRAS*, 516, 4922, doi: [10.1093/mnras/stac2557](https://doi.org/10.1093/mnras/stac2557)
- Roberts, Jr., W. W., Huntley, J. M., & van Albada, G. D. 1979, *ApJ*, 233, 67, doi: [10.1086/157367](https://doi.org/10.1086/157367)
- Rodriguez-Gomez, V., Snyder, G. F., Lotz, J. M., et al. 2019, *MNRAS*, 483, 4140, doi: [10.1093/mnras/sty3345](https://doi.org/10.1093/mnras/sty3345)
- Rossi, E. M., Stone, N. C., Law-Smith, J. A. P., et al. 2021, *SSRv*, 217, 40, doi: [10.1007/s11214-021-00818-7](https://doi.org/10.1007/s11214-021-00818-7)
- Salim, S. 2014, *Serbian Astronomical Journal*, 189, 1, doi: [10.2298/SAJ1489001S](https://doi.org/10.2298/SAJ1489001S)
- Sazonova, E., Morgan, C., Balogh, M., et al. 2024, *The Open Journal of Astrophysics*, 7, 77, doi: [10.33232/001c.123524](https://doi.org/10.33232/001c.123524)
- Shimakawa, R., Tanaka, M., Ito, K., & Ando, M. 2024, *PASJ*, 76, 191, doi: [10.1093/pasj/psae002](https://doi.org/10.1093/pasj/psae002)
- Shimizu, T. T., Mushotzky, R. F., Meléndez, M., Koss, M., & Rosario, D. J. 2015, *MNRAS*, 452, 1841, doi: [10.1093/mnras/stv1407](https://doi.org/10.1093/mnras/stv1407)
- Simard, L., Mendel, J. T., Patton, D. R., Ellison, S. L., & McConnachie, A. W. 2011, *ApJS*, 196, 11, doi: [10.1088/0067-0049/196/1/11](https://doi.org/10.1088/0067-0049/196/1/11)
- Sormani, M. C., Sobacchi, E., Fragkoudi, F., et al. 2018, *MNRAS*, 481, 2, doi: [10.1093/mnras/sty2246](https://doi.org/10.1093/mnras/sty2246)
- Sparre, M., & Springel, V. 2016, *MNRAS*, 462, 2418, doi: [10.1093/mnras/stw1793](https://doi.org/10.1093/mnras/stw1793)
- Stone, N. C., Vasiliev, E., Kesden, M., et al. 2020, *SSRv*, 216, 35, doi: [10.1007/s11214-020-00651-4](https://doi.org/10.1007/s11214-020-00651-4)
- Strauss, M. A., Weinberg, D. H., Lupton, R. H., et al. 2002, *AJ*, 124, 1810, doi: [10.1086/342343](https://doi.org/10.1086/342343)
- Tanaka, M., Koike, M., Naito, S., et al. 2023, *PASJ*, 75, 986, doi: [10.1093/pasj/psad055](https://doi.org/10.1093/pasj/psad055)
- Thorp, M. D., Bluck, A. F. L., Ellison, S. L., et al. 2021, *MNRAS*, 507, 886, doi: [10.1093/mnras/stab2201](https://doi.org/10.1093/mnras/stab2201)
- Toomre, A. 1977, in *Evolution of Galaxies and Stellar Populations*, ed. B. M. Tinsley & R. B. G. Larson, D. Campbell, 401
- Toomre, A., & Toomre, J. 1972, *ApJ*, 178, 623, doi: [10.1086/151823](https://doi.org/10.1086/151823)
- van Velzen, S., Gezari, S., Cenko, S. B., et al. 2019, *ApJ*, 872, 198, doi: [10.3847/1538-4357/aafe0c](https://doi.org/10.3847/1538-4357/aafe0c)
- van Velzen, S., Gezari, S., Hammerstein, E., et al. 2021, *ApJ*, 908, 4, doi: [10.3847/1538-4357/abc258](https://doi.org/10.3847/1538-4357/abc258)
- Verwilghen, P., Emsellem, E., Renaud, F., et al. 2024, *A&A*, 687, A53, doi: [10.1051/0004-6361/202348772](https://doi.org/10.1051/0004-6361/202348772)
- Walmsley, M., Géron, T., Kruk, S., et al. 2023, *MNRAS*, 526, 4768, doi: [10.1093/mnras/stad2919](https://doi.org/10.1093/mnras/stad2919)

- Wang, J., & Merritt, D. 2004, *ApJ*, 600, 149,
doi: [10.1086/379767](https://doi.org/10.1086/379767)
- Weinberger, R., Springel, V., Hernquist, L., et al. 2017,
MNRAS, 465, 3291, doi: [10.1093/mnras/stw2944](https://doi.org/10.1093/mnras/stw2944)
- Wevers, T., van Velzen, S., Jonker, P. G., et al. 2017,
MNRAS, 471, 1694, doi: [10.1093/mnras/stx1703](https://doi.org/10.1093/mnras/stx1703)
- Wevers, T., Stone, N. C., van Velzen, S., et al. 2019,
MNRAS, 487, 4136, doi: [10.1093/mnras/stz1602](https://doi.org/10.1093/mnras/stz1602)
- Wilkinson, S., Ellison, S. L., Bottrell, C., et al. 2024,
MNRAS, 528, 5558, doi: [10.1093/mnras/stae287](https://doi.org/10.1093/mnras/stae287)
- Wilkinson, S., Ellison, S. L., Bottrell, C., et al. 2022,
MNRAS, 516, 4354, doi: [10.1093/mnras/stac1962](https://doi.org/10.1093/mnras/stac1962)
- Wong, T. H. T., Pfister, H., & Dai, L. 2022, *ApJL*, 927,
L19, doi: [10.3847/2041-8213/ac5823](https://doi.org/10.3847/2041-8213/ac5823)
- Yao, Y., Ravi, V., Gezari, S., et al. 2023, *ApJL*, 955, L6,
doi: [10.3847/2041-8213/acf216](https://doi.org/10.3847/2041-8213/acf216)
- York, D. G., Adelman, J., Anderson, Jr., J. E., et al. 2000,
AJ, 120, 1579, doi: [10.1086/301513](https://doi.org/10.1086/301513)
- Zurita, A., Relaño, M., Beckman, J. E., & Knapen, J. H.
2004, *A&A*, 413, 73, doi: [10.1051/0004-6361:20031049](https://doi.org/10.1051/0004-6361:20031049)

APPENDIX

A. THE 14 SDSS TDES' MORPHOLOGICAL PARAMETERS

In this section, we show the morphological parameters of our TDE host galaxies in Table. A.1.

i	TDE	$C_{\text{stat,UNIONS}}$	$C_{\text{stat,SDSS}}$	C	$A_{\text{stat,UNIONS}}$	$A_{\text{stat,SDSS}}$	R_A	V_{MUMMI}
1	ASASSN-14ae	3.35263	3.08042	0.496	0.017033	0.007253	0.016	0
2	ASASSN-14li	-	3.07758	0.747	-	0.044505	0.009	2
3	AT2018hyz	-	2.95760	0.433	-	0.106074	0.006	0
4	AT2019azh	-	4.33293	0.526	-	0.053525	0.030	0
5	AT2018dyk	3.35835	3.22714	0.296	0.108391	0.035370	0.042	0
6	AT2020ocn	3.38016	2.89894	0.411	0.010670	-0.014597	0.010	0
7	AT2020wey	-	3.22147	0.470	-	-0.010219	0.014	-
8	PTF09ge	3.64364	3.16977	0.413	0.017687	-0.018834	0.020	0
9	RBS1032	-	2.70987	0.476	-	0.025407	0.017	-
10	SDSSJ0748	2.60593	2.73312	0.409	0.003300	0.006259	0.015	0
11	SDSSJ1323	3.65326	3.29657	0.509	0.019084	-0.063164	0.015	0
12	SDSSJ1342	-	2.88064	0.445	-	-0.001452	0.023	0
13	SDSSJ1350	4.07896	4.20559	0.385	0.042012	-0.007431	0.013	0
14	iPTF15af	-	3.19621	0.353	-	-0.020717	0.012	0

Table A.1. Morphological parameters of the 14 SDSS TDEs. The parameters (from left to right) are: index i , TDE name, STATMORPH concentration measured using UNIONS image $C_{\text{stat,UNIONS}}$, STATMORPH concentration measured using SDSS image $C_{\text{stat,SDSS}}$, concentration measurement from L. Simard et al. (2011) C , STATMORPH asymmetry measured using UNIONS image $A_{\text{stat,UNIONS}}$, STATMORPH asymmetry measured using SDSS image $A_{\text{stat,SDSS}}$, residual asymmetry R_A from L. Simard et al. (2011), and MUMMI's number of vote (out of 20 models) for merger identification V_{MUMMI} .

B. ERROR PROPAGATION

In this section, we detail the error calculations used in Fig. 5, and 6. Unfortunately, the morphological measurement does not technically come with uncertainties. We estimate the uncertainty of an individual measurements σ_m based on E. Sazonova et al. (2024), taking the root mean squared error of the asymmetry measurements from pairs of observations of the same galaxy from images of similar depth as our typical uncertainty.

The weighted mean is

$$\bar{X}_{\text{control}} = \frac{\sum_j w_j \cdot X_{\text{control},j}}{\sum_j w_j}, \quad (\text{B1})$$

with a weighted variance;

$$\sigma_w^2 = \frac{\sum_j w_j \cdot (X_{\text{control},j} - \bar{X}_{\text{control}})^2}{\sum_j w_j}. \quad (\text{B2})$$

and thus the standard error of mean is

$$\sigma_{\text{SEM}}^2 = \frac{\sum_j w_j^2 \sigma_w^2}{(\sum_j w_j)^2}. \quad (\text{B3})$$

The difference between the TDE host and its controls is

$$\Delta X = X_{\text{TDE}} - \bar{X}_{\text{control}}. \quad (\text{B4})$$

Hence, it has an uncertainty of

$$\sigma_{\Delta X}^2 = \sigma_m^2 + \sigma_{\text{SEM}}^2 \quad (\text{B5})$$

C. OTHER MEASURES OF ASYMMETRY AND CONCENTRATION

We also include the analysis for the concentration C (c1.g) and residue asymmetry R_A (ra1.3.g) from L. Simard et al. (2011) as a function of M_{BH} , M_* , and z here in Fig. C.1.

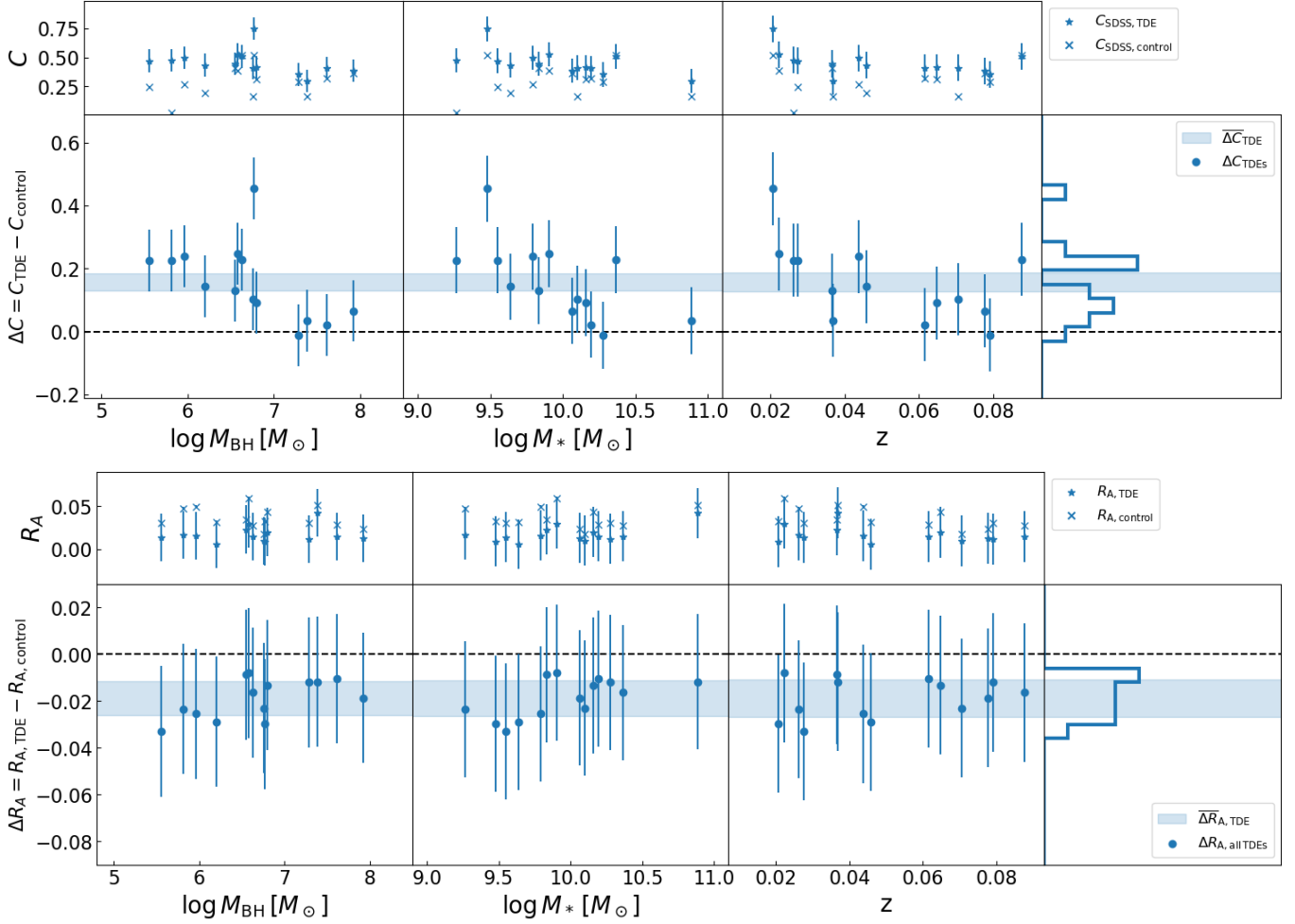


Figure C.1. The same analysis in Sec. 3.2 on the concentration C (top) and residual asymmetry R_A (bottom) from L. Simard et al. (2011). The symbols remain the same style as Fig.5. These measurements are done using SDSS images only, hence only in blue. Asymmetries are not enhanced (slightly suppressed) and concentrations are enhanced in TDE hosts relative to controls. These outcomes agree qualitatively our results using STATMORPH measurements.